HIGH PERFORMANCE LONG-WAVE INFRARED (LWIR) HGCDTE ON SILICON

SBIR Phase I

Contract Number: **W15P7T-05-C-H201**

Final Report

Reporting period: December 13, 2004 – June 15, 2005

EPIR Technologies Inc.

Program Manager: Chris Grein
Email: grein@epir.com
Mobile: 630-248-7441

Principal Investigator: Paul Boieriu
Email: pboieriu@epir.com
Mobile: 630-842-0893

590 Territorial Drive, Unit B
Bolingbrook, IL 60440
Phone: 630-771-0203
Fax: 630-771-0204

REPORT DOCUMENTATION PAGE

Form Approved
OMB No. 0704-0188

1. REPORT DATE *(DD-MM-YYYY)*	2. REPORT TYPE	3. DATES COVERED *(From - To)*
06-06-2005	Final	12/13/04 – 06/15/05

4. TITLE AND SUBTITLE

High Performance Long-wave Infrared (LWIR) HgCdTe on Silicon

5a. CONTRACT NUMBER
W15P7T-05-C-H201

5b. GRANT NUMBER

5c. PROGRAM ELEMENT NUMBER

6. AUTHOR(S)
Dr. Paul Boieriu
Dr. Chris Grein

5d. PROJECT NUMBER

5e. TASK NUMBER

5f. WORK UNIT NUMBER

7. PERFORMING ORGANIZATION NAME(S) AND ADDRESS(ES)
EPIR Technologies Inc., 590 Territorial Dr, Suite B,
Bolingbrook, IL 60440

8. PERFORMING ORGANIZATION REPORT NUMBER

9. SPONSORING / MONITORING AGENCY NAME(S) AND ADDRESS(ES)

Commander US Army CECOM, ACQ Center
AMSEL-ACCB-RT-Z
Fort Monmouth, NJ 07703-5008

10. SPONSOR/MONITOR'S ACRONYM(S)

11. SPONSOR/MONITOR'S REPORT NUMBER(S)

12. DISTRIBUTION / AVAILABILITY STATEMENT

Distribution Statement A: Approved for public release; distribution is unlimited

13. SUPPLEMENTARY NOTES

14. ABSTRACT

It is critical in the field of infrared imaging to reduce focal plane array costs and simultaneously improve their performance. The use of long wavelength infrared HgCdTe grown on Si substrates will reduce array costs, increase their mechanical strength and permit the fabrication of larger area arrays than possible with present-day technology based on bulk CdZnTe substrates. Performance enhancements result from the passivation of defects created by the lattice mismatch between HgCdTe and Si. We are developing a reliable method to passivate the electrical activity of defects such as dislocations in long-wavelength HgCdTe grown on Si. We demonstrated increases in carrier recombination lifetimes and mobilities as a consequence of defect passivation with hydrogen, and showed that the passivation is stable over time.

15. SUBJECT TERMS

16. SECURITY CLASSIFICATION OF:			17. LIMITATION OF ABSTRACT	18. NUMBER OF PAGES	19a. NAME OF RESPONSIBLE PERSON
UNCLASSIFIED					Sivalingam Sivananthan
a. REPORT	b. ABSTRACT	c. THIS PAGE			19b. TELEPHONE NUMBER *(include area code)*
(U)	(U)	(U)	200		630-771-0201

Standard Form 298 (Rev. 8-98)
Prescribed by ANSI Std. 239.18

Table of contents

Tables

Figures

Introduction

Current state-of-the-art infrared focal plane arrays (IRFPAs) are based on HgCdTe material epitaxially grown on bulk CdZnTe substrates, and use a hybrid technology in which HgCdTe detector arrays and Si readout chips are fabricated separately and connected element by element using indium bumps. The size of these IRFPAs is limited by the size of the available CdZnTe substrates and the thermal mismatch between CdZnTe and the Si readout circuit (thermal expansion coefficients: 4.8×10^{-6} K^{-1} and 2.3×10^{-6} K^{-1}, respectively), which misaligns the photodiodes with respect to the Si circuit during heating and cooling cycles. Additionally, impurities in the bulk CdZnTe material can degrade system performance, and the overall mechanical strength of the substrate can be a serious concern. Having HgCdTe fabricated on Si-based composite substrates would eliminate the aforementioned drawbacks related to the HgCdTe/CdZnTe system. Indeed, the use of Si-based substrates would also lower detector costs and permit the realization of larger area arrays.

Molecular beam epitaxy (MBE) has emerged in recent years as the flexible manufacturing technology for IRFPA materials offering the greatest control. The superiority of the MBE growth technology is enhanced further by the possibility of growing HgCdTe on alternate, robust and inexpensive substrates such as silicon. Over the past decade, several research and development groups, including EPIR Technologies Inc., the Microphysics Laboratory (MPL) at the University of Illinois at Chicago, the Night Vision Laboratory (NVL), the Army Research Laboratory (ARL), Rockwell Scientific and Hughes Research Laboratory (HRL), have carried out intensive research on the growth of CdTe on Si by MBE. As a result of this community-wide effort, CdTe/Si has reached a level of maturity to compete with bulk CdZnTe as a substrate for SWIR and MWIR HgCdTe applications. A MWIR 1024 x 1024 IRFPA based on HgCdTe/Si grown at EPIR has been fabricated by Rockwell Scientific.

When CdTe/Si(211) is used as a substrate for the molecular beam epitaxial growth of $Hg_{0.78}Cd_{0.22}Te$, a lattice mismatch of 0.28% exists between the HgCdTe and CdTe. Such a lattice mismatch, although small, induces dislocations in the HgCdTe layer

when the layer thickness is greater than the critical thickness, which in this case is less than 200 nm. This translates into a dislocation density of about 10^9 cm^{-2} at the HgCdTe/CdTe interface, which leads to dislocation densities typically in the 10^6 cm^{-2} range at the top of the HgCdTe surface after growth to a thickness of about 10 μm. Although such dislocation densities have proven satisfactory for many SWIR and MWIR applications, they are unacceptable for LWIR applications under low temperature and low background conditions. Note that the large lattice mismatch between CdTe and Si may also lead to dislocations that thread into the HgCdTe epilayers. Dislocations in the HgCdTe can shunt p-n junctions, act as carrier recombination centers and reduce carrier mobilities.

One possible solution is to reduce the dislocation density in HgCdTe grown on Si by employing a lattice-matched composite substrate rather than CdTe/Si. $Cd_{1-x}Zn_xTe$/Si, in which the lattice constant can be tailored to exactly match that of the HgCdTe by varying the Zn composition, would be a natural choice for this new substrate. Four per cent Zn in $Cd_{1-x}Zn_xTe$ is required to achieve lattice matching with the LWIR material $Hg_{0.78}Cd_{0.22}Te$. However, the MBE growth of $Cd_{1-x}Zn_xTe$ on Si proves to be much more challenging than the growth of CdTe on Si. In addition to the defects created in CdTe or $Cd_{1-x}Zn_xTe$ by their large lattice mismatch (19%) with Si, the crystalline quality of MBE-grown $Cd_{1-x}Zn_xTe$ degrades significantly as the Zn concentration increases for even small amounts of Zn. Thus, the use of $Cd_{1-x}Zn_xTe$/Si substrates for the MBE growth of HgCdTe would lead to serious problems requiring extensive research to overcome.

We implemented a second solution, namely growing LWIR HgCdTe on CdTe/Si substrates despite the resultant high dislocation densities, but passivating the dislocations to improve device performance. This was achieved through the introduction of an impurity atomic species that passivates the dangling bonds created by the dislocations. Hydrogen has been most extensively utilized for such passivation. The passivation mechanism is straightforward: the dangling bonds give rise to states in the bandgap that act as Shockley-Read-Hall recombination centers. However, the attachment of the impurity atomic species to the dangling bond eliminates the gap states, forming bonding and antibonding states. The bonding states drop into the valence band, while the

unoccupied antibonding states are lifted into the conduction band, so that neither are electrically active.

The hydrogen passivation of both shallow and deep levels has been well studied in many major semiconductors, particularly Si and GaAs. Perhaps, its most prominent application is in a-Si:H solar cells. Notably, it has been found to significantly reduce leakage currents through dislocation cores in GaN [1]. Indeed, atomic hydrogen has been found to passivate shallow donors and acceptors in virtually all semiconductors. Extensive theoretical and experimental studies have in many cases elucidated the microscopic mechanisms of shallow level passivation. Deep level passivation has been found to be more thermally stable than shallow, and hence is thought to have greater practical utility. Even so, the thermal stability has generally not been found to be so great as to make hydrogen passivation a major tool for the fabrication of high performance semiconductor-based devices. The exact mechanisms by which hydrogen passivates deep levels are poorly understood, in part due to the lack of a clear understanding of the microscopic nature of many deep levels. Defect–hydrogen complexes may involve several hydrogen atoms and host-lattice structural rearrangements.

The passivation of shallow and deep levels in CdTe and CdZnTe has received some attention [2-4]. As in most group IV and III-VI semiconductors, hydrogen has been generally found to be an effective passivant when introduced in either molecular or atomic form, with resulting improvements in electrical and optical properties.

The hydrogen passivation of HgCdTe has received only superficial study. Early research involved electrochemical methods of introducing hydrogen into $Hg_{0.5}Cd_{0.5}Te$ followed by deep level transient spectroscopy to determine the influence on deep levels [5, 6]. The dominant deep levels at approximately $E_g/2$ and $3E_g/4$ were significantly reduced in concentration after hydrogenation. Unfortunately, annealing at 70°C restored their activity. Clearly, the passivation of deep-level defects must be stable to be useful, whereas any passivation of dopants should be unstable so as not to inhibit their activity. Two more recent papers [7,8] examine mercury-vacancy doped MWIR and LWIR HgCdTe. Ref. [7] reaches the conclusion that Electron Cyclotron Resonance (ECR) plasma hydrogenation is effective in passivating surface trap states, whereas ref. [8]

concludes that its only role was to passivate mercury vacancies. It has also been found that hydrogenation improves the quality of HgCdTe/passivant interfaces [9].

Some studies have concluded that dislocations decrease the minority carrier lifetimes [10,11] and carrier mobilities [12] of HgCdTe. It is interesting to note that some HgCdTe/CdTe/Si layers grown at EPIR Technologies and U. Illinois at Chicago have shown lifetimes comparable to those grown on CdZnTe. Indeed, a recent work [13] also reports the recombination lifetimes of two samples of LWIR HgCdTe on Si to be comparable to those grown on CdZnTe, even though the dislocation densities are greater. The authors of [13] conjecture that this may be a consequence of not all dislocations being active as recombination centers. The reproducibility of these results and the lifetime uniformity over the area of the wafers is not clear. Note that the authors of ref. [13] do observe a drop in mobility with increasing dislocation density, in qualitative agreement with those of ref. [12]. The above literature survey on the hydrogen passivation of HgCdTe reveals many inconsistencies between the results of various groups. Even though there are some indications that lifetimes for HgCdTe on Si can be comparable to those on CdZnTe, defect passivation promises an improvement in the reproducibility of these results as well as creating uniform lifetimes over large area wafers, leading to greater yields than those currently reached. Furthermore, passivation holds the promise of preventing dislocations from shunting currents in photodiode junctions. It is part of the goal of this effort to establish a portable and reliable scheme for the passivation of dislocations, so as to make it possible for different groups to obtain consistent and reproducible results.

Experimental Approach

Our experimental approach consisted of testing basic material properties that are relevant to infrared device performance on samples and devices that are bulk-passivated with atomic hydrogen, and comparing these material properties with those of un-passivated samples.

Annealed and as-grown samples of 10mmx10mm size were exposed to ECR plasmas of various characteristics. With one exception, samples were covered with thin ZnS layers prior to ECR exposure. After hydrogen exposure, the samples were cut into 5mm x 5mm pieces and used for minority carrier lifetime and Hall measurements to test the effects of bulk passivation with hydrogen. Similar measurements were performed after shelving the samples for more than 30 days, as well as after heating several samples at 80 °C for 40 min. to explore the stability of hydrogen passivation. Should an Option Period be awarded, we plan to fabricate planar photodiodes from epilayers that were exposed to hydrogen and compare them with devices that were not hydrogen-passivated.

Three 3" HgCdTe/Si wafers were used as part of the Phase I effort. Figure 1 shows the FTIR spectra of the three wafers measured at room temperature.

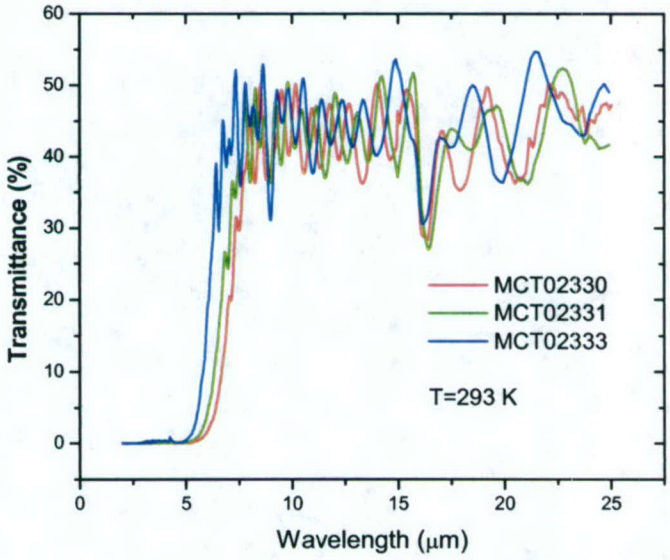

Figure 1. FTIR spectra of three LWIR-sensitive HgCdTe heterostructure wafers

The FTIR spectra show sharp cut-offs within the MWIR range at room temperature (hence are LWIR at low temperatures-see Table 1) and uniform transmittances over large spectral ranges, indicating the high quality of these epilayers.

The layer structure of the three wafers is shown in Figure 2. This is the typical heterostructure used by EPIR Technologies Inc. for p-on-n double layer heterojunction (DLHJ) devices in which the p-type layer is formed by post-growth As ion implantation. All of the heterostructure layers, with the exception of the buffer, were in situ doped with indium.

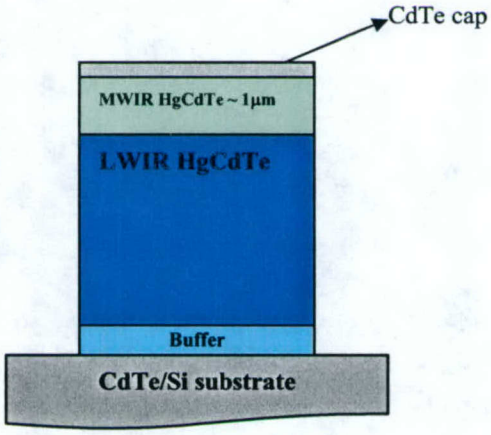

Figure 2. Cross-sectional schematic of the employed LWIR heterostructure

The LWIR absorbers in the samples had similar thicknesses, approximately 14 microns, and were doped with In to produce n-type conduction with carrier concentrations in the 1-5x10^{15} cm^{-3} range.

Samples of 5mmx5mm size were cut from the three wafers (MCT02330, MCT02331 and MCT02333) and measurements were performed on the as-grown samples to establish basic material properties. They are shown in Table 1. Note that high EPD samples were chosen for this study to help provide definitive evidence of the effects of hydrogen passivation. EPIR Technologies' best HgCdTe/Si layer has an EPD of 1 x 10^6 cm^{-2}, with typical values being 3-5 x 10^6 cm^{-2}.

Table 1. Characteristics of samples

Sample name	EPD (cm^{-2})	Cadmium composition x	Cutoff at 77K* (μm)	Cutoff at 293 K (μm)
MCT02330	1.89×10^7	0.212	12.1	7.3
MCT02331	6.10×10^6	0.214	11.7	7.2
MCT02333	8.44×10^6	0.234	9.0	6.2

* extrapolated from room temperature data using Hansen, Schmitt, Casselman formula (G. L. Hansen, J. L. Schmitt, and T. N. Casselman, J. Appl. Phys. **53**, 7099 (1982))

Additional samples of 5mmx5mm size were also cut from the three wafers and annealed. These were used as reference samples to determine the pre-ECR characteristics. The temperature profile used during annealing was the same as that used for achieving As activation. Namely, the sample temperature was kept at 425 °C for 10 minutes during the first stage, followed by a longer second stage during which the sample was kept at 235°C. The Hg droplet temperature was kept 5 °C below the sample temperature at all times during annealing.

A brief description of the employed closed-tube annealing process is given below. Approximately 9"-long quartz ampoules with bottlenecks about 3-in. from one end were used to hold samples and Hg droplets. Two sizes of cylindrical ampoules were typically used. One has inner (ID) and outer diameters (OD) of 9mm and 16 mm, respectively. The second has ID and OD of 12 mm and 16 mm, respectively. Following a degreasing step, the ampoules were etched before rinsing with a hydrofluoric acid solution (HF:DI, 1:19) for about 5 minutes. The ampoules were constantly shaken to allow the solution to flow through the bottlenecks. A thorough rinsing with DI water terminated the cleaning procedure. The ampoules were then loosely wrapped in Al foil and baked for 1 hour at 500 °C. Once cooled, each ampoule was first loaded with a Hg droplet of about 4 ml volume, and then with the sample. The bottleneck prevented the sample from being in contact with the Hg during the sealing of the ampoule. The ends of each ampoule were sealed by melting and collapsing the ampoule walls with an H_2/O_2 flame (quartz melts at around 1300 °C). The ampoules were mounted using a compression fitting to a manifold that permitted pumping and purging with Ar. Pumping was done using a liquid nitrogen-cooled sorption pump. A thermocouple pressure gauge was used to measure the pressure.

After sealing, each sample was brought from the bottleneck to the end of the ampoule by tapping the ampoule. As a consequence, the Hg droplet and the sample were located at opposite ends of each ampoule. Sealed ampoules containing both Hg and a sample were then placed in a multizone furnace. The ampoules were balanced on a fire brick to allow the samples and the Hg droplets to be exposed to different temperatures. The pressure within the ampoule is principally determined by the partial pressure of saturated Hg vapor at the set temperature. Following the thermal treatment, the ampoules were rapidly quenched in a cold water bath for about 10-15 min. The sealed ampoules were then cut open and the samples retrieved.

Results and Discussions

Investigation of hydrogen incorporation

Twelve 10mmx10mm samples were prepared for ECR high-density plasma hydrogenation. Eight (MCT02330c3, MCT02330c11, MCT02331c6, MCT02331c12, MCT02331c13, MCT02333c3, MCT02333c11, MCT02333c17) were annealed and capped with ZnS, one (MCT02330c10) was annealed but without a ZnS cap, and one (MCT02330c7) was capped with ZnS but not annealed. Two samples consisted of fully processed devices (dev and dev_m). Devices were included in the first ECR batch in order to observe the ECR plasma's influence on device passivation and on the metal contacts.

An ECR process based on H_2 with a low d.c. bias was chosen to avoid physical damage by the plasma. The excited species generated in the ECR region are used to dissociate and ionize molecular hydrogen. The process is designed to provide both atomic and ionized hydrogen. The hydrogen is expected to act as a passivant.

Table 2 summarizes the ECR conditions employed with these samples.

Table 2. ECR conditions used for the first batch of samples

Sample ID	H2 flow (sccm)	Ar flow (sccm)	Pressure (mTorr)	MW Power (watts)	DC bias power (watts)	Temperature (°C)	Duration (min)
MCT02330c3	20	0	0.4	450	0	24	10
MCT02330c7	20	0	0.4	450	60	60	10
MCT02330c10	20	0	0.4	450	0	60	10
MCT02330c11	20	0	0.4	450	0	60	15
MCT02331c6	20	0	2.0	450	0	60	10
MCT02331c12	20	0	10.0	450	0	60	10
MCT02331c13	20	80	2.0	300	60	60	1
MCT02333c3	4	16	0.4	450,350	0	60	3,7
MCT02333c11	20	0	0.4	450	0	60	10
MCT02333c17	20	80	2.0	300	60	24	1
dev	20	0	0.4	450	0	60	10
dev_m	20	0	0.4	450	0	60	10

SIMS measurements were performed on four samples (MCT02330c3C, MCT02330c10C, MCT02331c6C, and MCT02331c6D) after being exposed to ECR. Samples MCT02330c3C and MCT02330c10C were selected to verify the presence of hydrogen following their exposure to different ECR conditions and sample preparations. While hydrogen clearly incorporated in sample MCT02330c10C (Figure 3), SIMS measurements on sample MCT02330c3C (Figure 4) showed hydrogen concentrations commensurate with the detection limit for most of the bulk sample, suggesting that hydrogen may have incorporated, but at concentrations below $4x10^{16}$ cm^{-3}. Please note that the depth scales in Figures 3 and 4 are not correct because ZnS, HgCdTe and CdTe have very different sputtering rates during SIMS. In both samples, the concentration of hydrogen was higher closer to the surface and diffusion tails were observed. Enhanced diffusion was noted for sample MCT02330c10C.

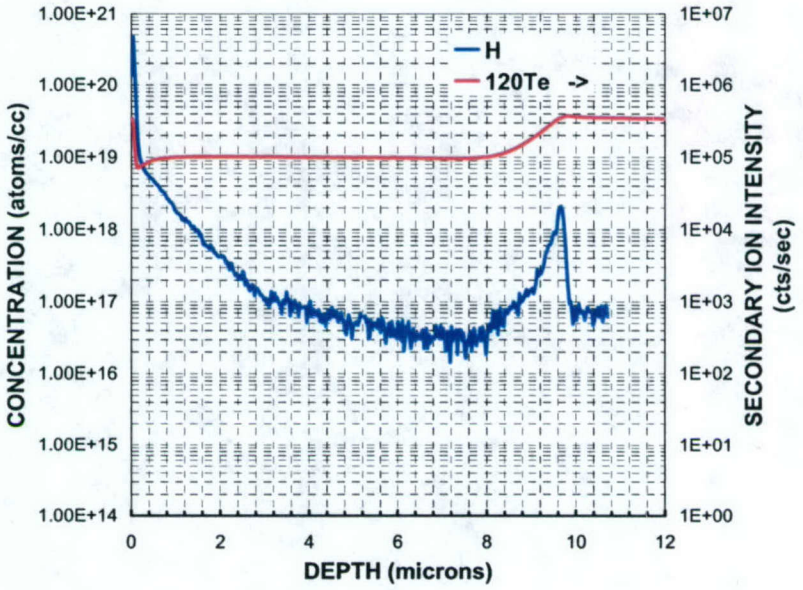

Figure 3. Hydrogen concentration in sample MCT02330c10C measured by SIMS.

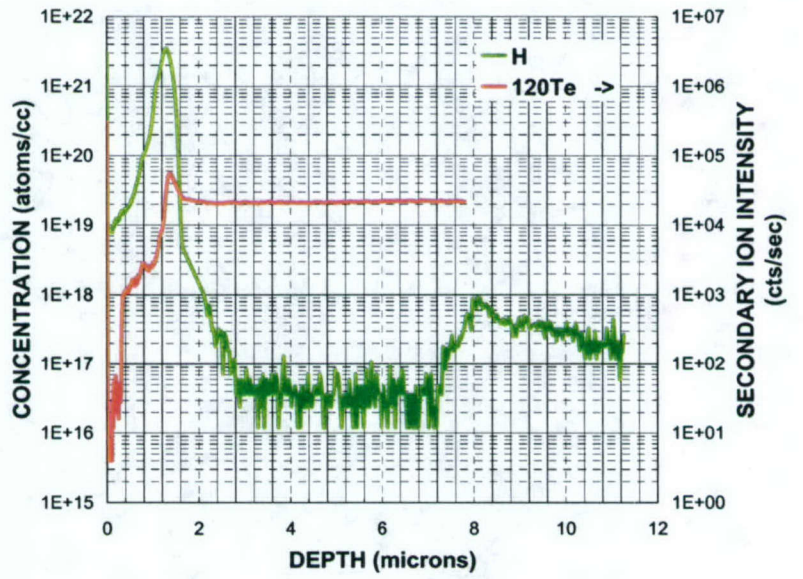

Figure 4. Hydrogen concentration in sample MCT02330c3C measured by SIMS.

In contrast, sample MCT02331c6C did not show a concentration of hydrogen above the SIMS detection limit (Figure 5). Although Figure 5 did not show measurable concentrations for hydrogen, one cannot rule out the possibility that hydrogen may have incorporated into the sample with an atomic concentration below $4x10^{16}$ cm^{-3}.

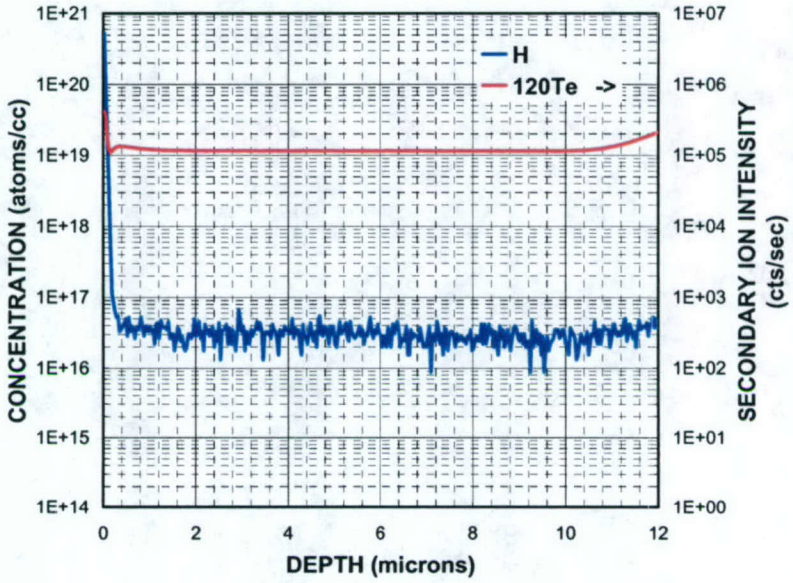

Figure 5. Hydrogen SIMS profile for sample MCT02331c6

Indeed, we estimate that a substantially lower concentration of hydrogen would be sufficient to passivate typical concentrations of dangling bonds associated with dislocations. A rough estimate of the density of dangling bonds (DBD) that could be available for bonding with hydrogen ions is:

$$\textbf{DBD} = 3xNx10^{6}\ cm^{-2} \times 4x10^{7}\ cm^{-1} = 12N \times 10^{13}\ cm^{-3} = 4.8 \times 10^{14}\ cm^{-3} \qquad \text{Eq. 1}$$

This estimate was obtained assuming a HgCdTe atomic density of 10^{23} cm^{-3}, and an EPD value of 10^{6} cm^{-2}. The number of atoms per unit length is ~ $4x10^{7}$ cm^{-1}. Other assumptions were that: (i) threading dislocations are parallel to the growth direction, (ii) that the dislocations are uniformly distributed, far apart and do not interact with each other, and (iii) that no other defects are formed along the threading dislocations. In equation 1, N represents the number of atoms in a plane perpendicular to a threading dislocation that are affected by its presence (Figure 6). We assumed each of these atoms has 3 dangling bonds due to the dislocation. We also assume that hydrogen is more likely

to be found in HgCdTe after bonding with such dangling bonds, and that interstitial hydrogen may be present but in lower concentrations.

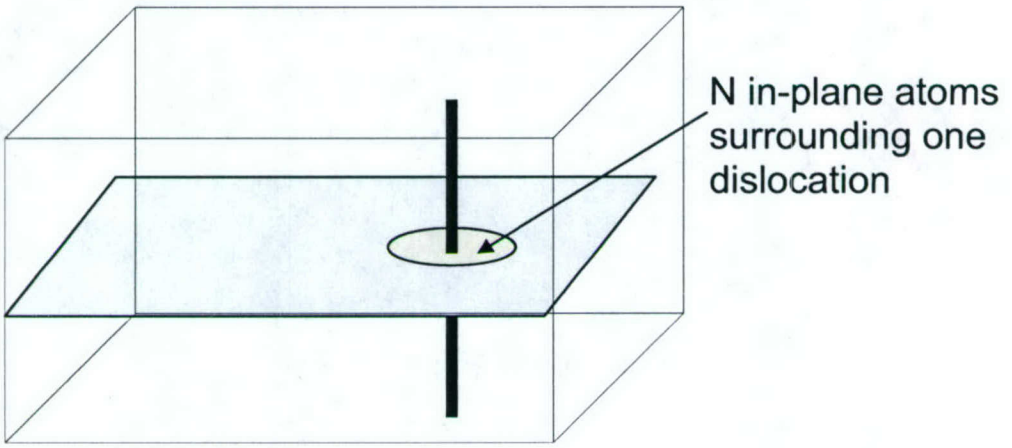

Figure 6. Sketch used in the estimation of dangling bonds density created by threading dislocations

The principal conclusion is that SIMS may not be able to detect the presence of the hydrogen for hydrogen concentrations commensurate with the density of dangling bonds. Note as well that hydrogen concentrations above those needed for dislocation passivation may be undesirable because of, for example, greater plasma-induced damage associated with generating high concentrations of hydrogen, and deleterious effects of interstitial hydrogen, if any.

Investigation of surface morphologies

Visual inspection indicated surface discolorations of the ZnS overlayer on two of the four layers. The color of ZnS was green prior to ECR exposure. This color was maintained after ECR for MCT02330c3 and MCT02330c11. In contrast, MCT02331c6 changed its color to purple, and MCT02333c17 changed its color into a lighter green. Both samples were exposed to similar pressures during the ECR process, higher than the pressures used for samples MCT02330c3 and MCT02330c11.

Similarly, a change in color was observed for sample MCT02330c10, which was not covered with ZnS. This indicates that the ECR plasma had reacted with the protective CdTe layer.

All samples that were exposed to the ECR plasma had to be cleaned in order to remove vacuum grease residue from mounting. The cleaning was performed using multiple baths of trichloroethylene, isopropyl alcohol and DI water. The samples were dried with nitrogen. During the cleaning process, the two samples that showed surface discolorations (MCT02331c6 and MCT02333c17) lost their ZnS coating either partially or entirely. Peeling of ZnS commenced during the trichloroethylene bath. For MCT02333c17, the entire ZnS layer was blown away during drying. Large patches of ZnS remained attached to sample MCT02331c6 even after drying. The difference between the two can be explained by the more aggressive ECR process that MCT02333c17 underwent. While increasing the microwave power is conducive to generating a higher density of ions within the plasma, a higher bias power can also enhance the density of hydrogen ions incorporated into the sample. As expected, the addition of Ar and the use of higher bias powers also increase the distress on the ZnS layer and promotes its peeling.

Optical microscopy was used to investigate the surface morphology of each of the samples discussed above, following most of the process steps. Figure 7 shows the surface morphologies of sample MCT02330c11. A slight deterioration is observed after annealing.

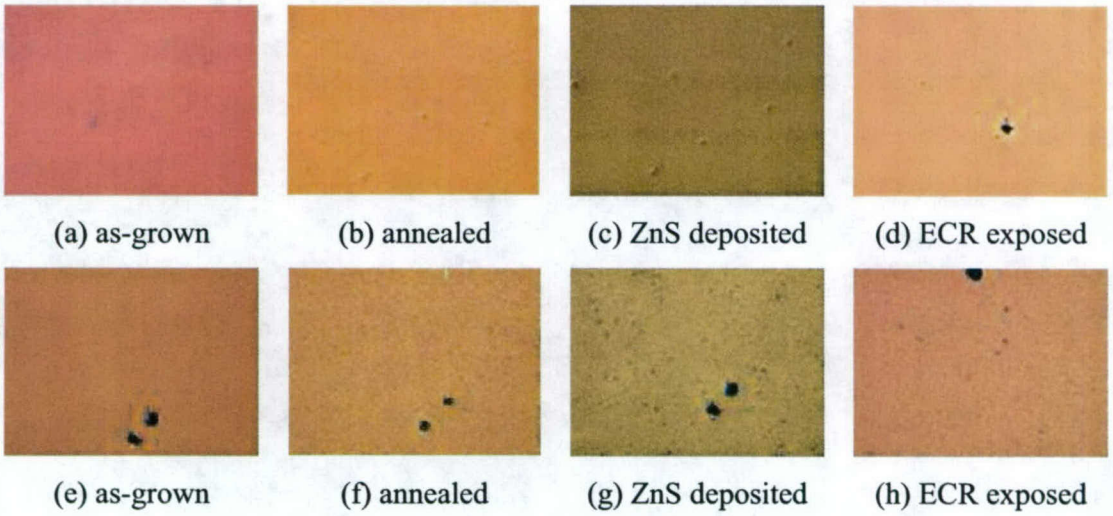

Figure 7. Surface morphology investigations of sample MCT02330c11 following various processes. Images were acquired with x100 magnification for a – d and with x500 magnification for e – h.

Figure 8 shows the surface morphologies of sample MCT02333c17. No obvious changes seemed to have occurred at a microscopic level during any of the shown process steps.

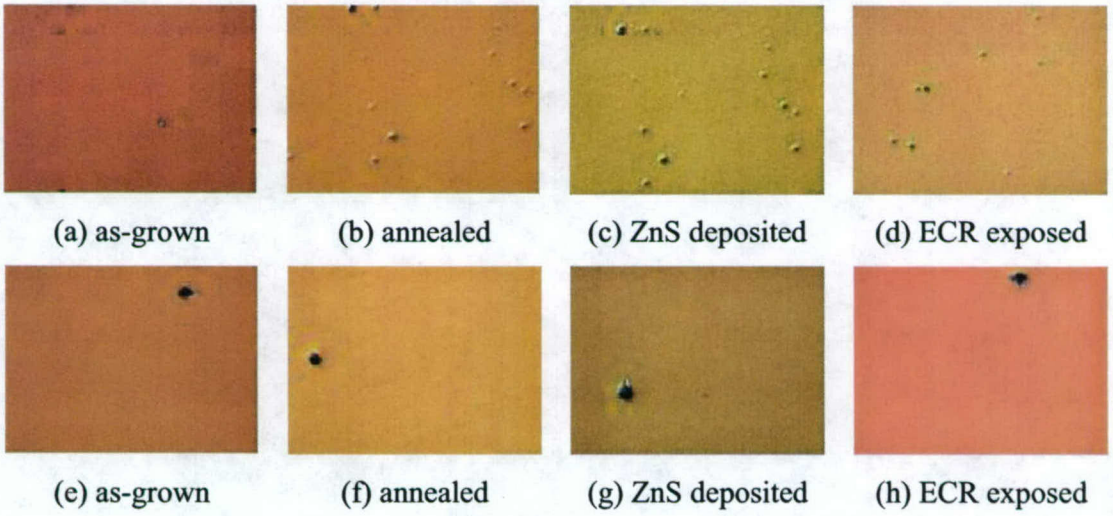

Figure 8. Surface morphology investigations of sample MCT02333c17 following various processes. Images were acquired with x100 magnification for a – d and with x500 magnification for e – h.

We also investigated the surface morphologies of two device samples (labeled here as "dev" and "dev_m"). They were both exposed with the ECR parameters mentioned by Jung et al. [7]. Figures 9 and 10 show the surface morphology of device samples prior to and after ECR exposure.

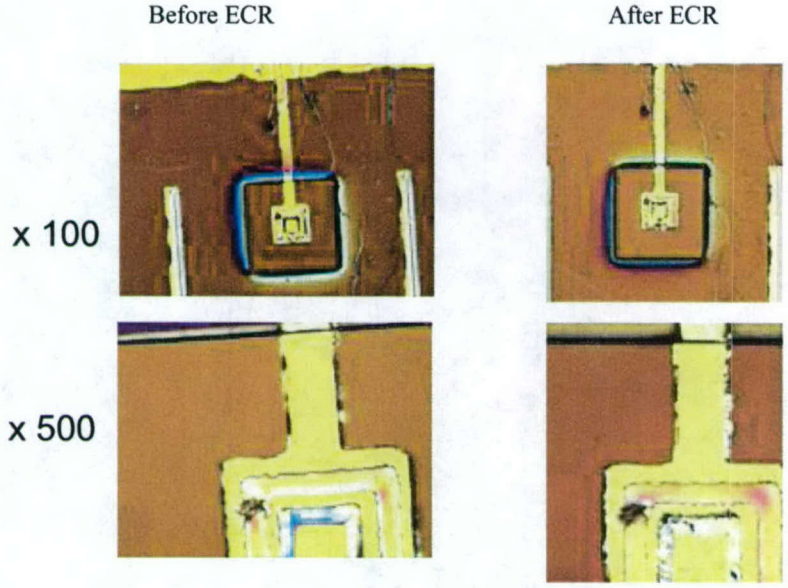

Figure 9. Surface morphology for device sample "dev" prior to ECR (left) and after ECR (right) for two magnifications

While no significant surface changes were observed for device sample "dev", that is not the case for device sample "dev_m". Figure 10 shows metal interconnects deterioration through the formation of blister-like features. We will continue to investigate the difference between the two behaviors and attempt further exposures of device samples.

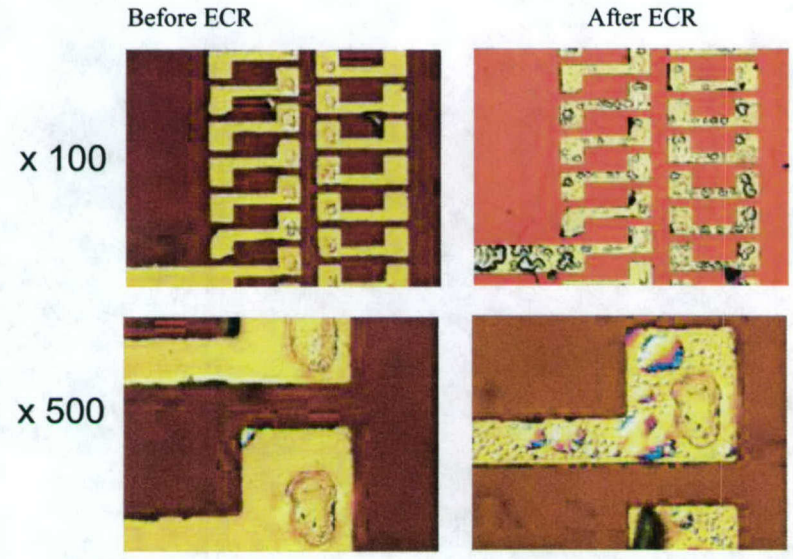

Figure 10. Surface morphology for device sample "dev_m" prior to ECR (left) and after ECR (right) for two magnifications

Electrical measurements

The ECR-exposed samples were each cut into four pieces of 5mmx5mm size. In order to preserve the density of defect-associated scattering centers, a photolithographic process was used to delineate cutting marks. Both the HgCdTe and CdTe layers were etched down to the silicon substrates along the cutting marks. In this way, the diamond blade used for cutting did not come in contact with the HgCdTe, minimizing the risk of damaging it, hence, minimizing the density of cutting-induced defects.

Hall electrical measurements were performed on ECR-exposed samples and reference samples that were annealed using a high temperature anneal (425 °C for 10 min) followed by a Hg vacancy-filling low temperature anneal at 235 °C for 24 hrs).

The photoconductive decay method was used to measure minority carrier lifetimes. A pulsed laser diode (with a peak wavelength of 850 nm and a pulse width less than 10 nsec) was used to illuminate the sample and excite carriers across the forbidden energy gap. Carrier recombination was monitored at different temperatures and the carrier lifetimes were extracted.

The Hall constants of all of the samples annealed at 425°C/235°C displayed an anomalous, nonmonotonic temperature dependence. When plotted as a function of the inverse temperature, the nonmonotonic curves could indicate one or more of the following: (i) the samples were exposed to insufficient Hg overpressure during annealing so Hg vacancies were created, leading to compensated conduction during Hall measurements, or (ii) the samples were exposed to sufficient Hg overpressure, yet post-anneal quenching or annealing-related diffusion of Hg and/or Te altered the conditions of the surfaces, creating regions with dissimilar defect levels, some of which are electrically active. In the second case, n^+/n or p/n layers could be formed. Even an essentially thin layer (skin layer) with a concentration of electrically active complexes (Te vacancies or interstitials, Hg vacancies or interstitials) different from that of the underlying epilayer could produce anomalous temperature dependences such as those seen in the Hall results. We speculate that such electrically active complexes were formed in samples from all three wafers (MCT02330, 2331 and 2333) during the 425°C/235°C anneal. Although an isotropic distribution of Hg vacancies (the entire HgCdTe volume contains a uniformly distributed density of vacancies, hence is compensated) could generate such anomalous results, we do not believe that to be the case for these samples due to the high values of the mobilities (Figures 12, 18, and 23).

By correlating the Hall data with EPD values, we concluded that threading dislocations may play an important role in the atomic diffusion processes that can take place during annealing and/or during ECR plasma exposure. Following ECR, we noticed that the electrically active complexes created during annealing were at least partially annihilated. All samples exhibited a change in their conduction properties with one exception (the Hall data for MCT02333c17 showed no significant change after ECR). It is not conclusive that plasma-generated hydrogen ions are responsible for the annihilation, but it is highly likely that the annihilation of such defects is due to the highly mobile H^+ ions. Based on Hall constant data, it appears that dislocations facilitate this annihilation process. Sample MCT02330 had the highest EPD and was the sample for which we observed the greatest change in conduction following ECR. In this sample, the low temperature conduction changed from p-type to n-type with low values of the Hall constant. When compared with the two samples that have lower EPD values, sample

MCT02330 appears to be "more" n-type than the other two. Samples MCT02333 and MCT02331 have higher Hall constants that are consistent with their EPD values. It is our conjecture that dislocations facilitated the diffusion of plasma ions, most likely hydrogen, into the HgCdTe samples.

Hall electrical measurements and minority carrier lifetime measurements were redone after shelf storage on samples MCT02330c3, MCT02333c11, MCT02333c3, and Hall measurements only redone on samples MCT02331c13 and MCT02333c17. Samples MCT02330c3 and MCT02331c13 were also heated at 80°C for 40 min. and their Hall properties were remeasured. We used the same contacts and leads for all measurements on a given sample.

Samples from wafer MCT02330

Figures 11 and 12 show the electrical carrier concentrations and carrier mobilities for those samples originating from wafer MCT02330.

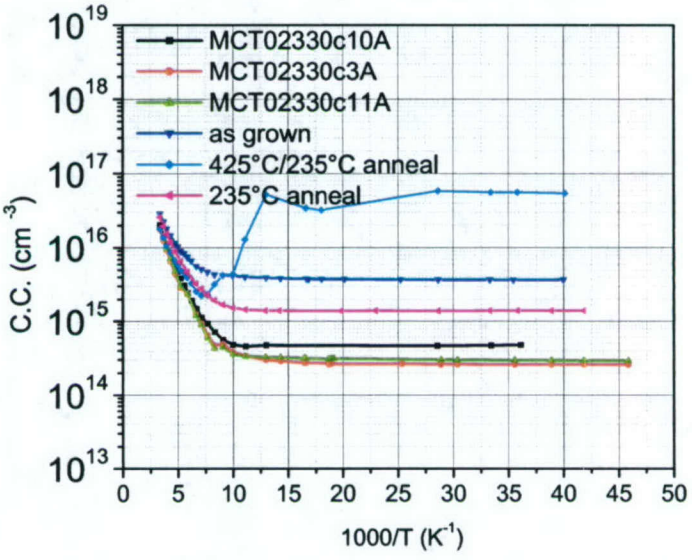

Figure 11. Hall carrier concentrations for samples from wafer MCT02330

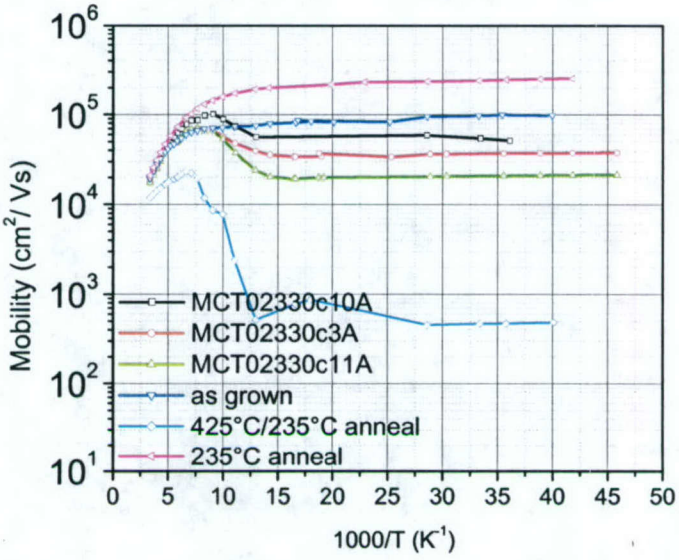

Figure 12. Hall mobilities for samples from wafer MCT02330

The measured temperature dependences of the Hall constants, which were used to determine both carrier concentrations and carrier mobilities, are shown in Figure 13.

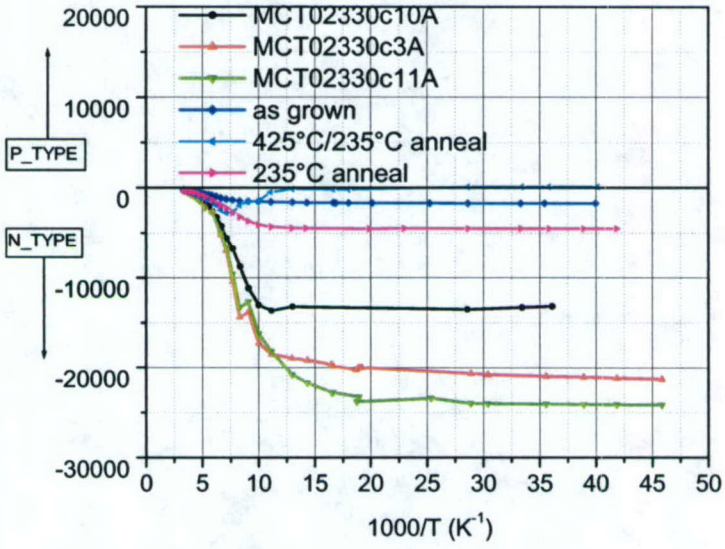

Figure 13. Hall constants Rh for samples from wafer MCT02330

Figures 14 and 15 show the carrier concentrations and mobilities for sample MCT02330c3 measured 86 days after the first Hall measurements and a total of 129 days

following the ECR exposure. In addition to investigating the effects shelf storage may have on electrical transport, we also tested the hydrogen passivation's stability after heating the sample to 80°C and maintaining this temperature for 40 min. This was performed 11 days after the second Hall measurement, a total of 140 days after ECR exposure. Hall measurement results following such experiments for sample MCT02330c3 are also shown in Figures 14 and 15.

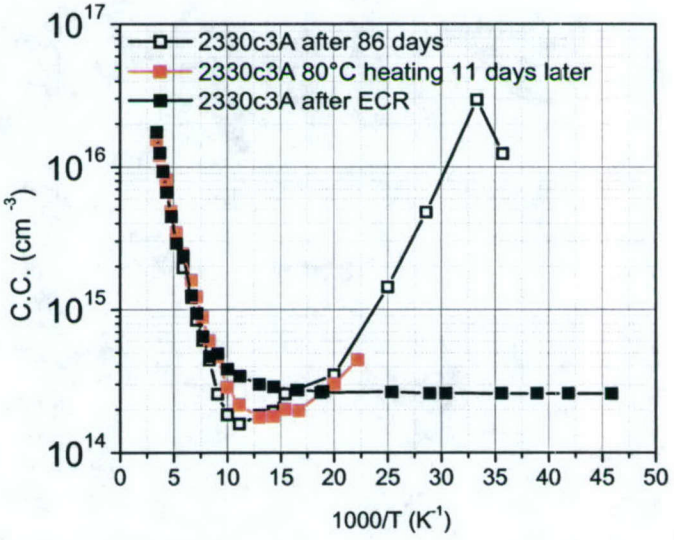

Figure 14. Hall electrical carrier concentrations measured 86 days apart for hydrogen passivated sample MCT02330c3. The red curve shows results from a measurement performed 11 days later, after heating the sample to 80°C.

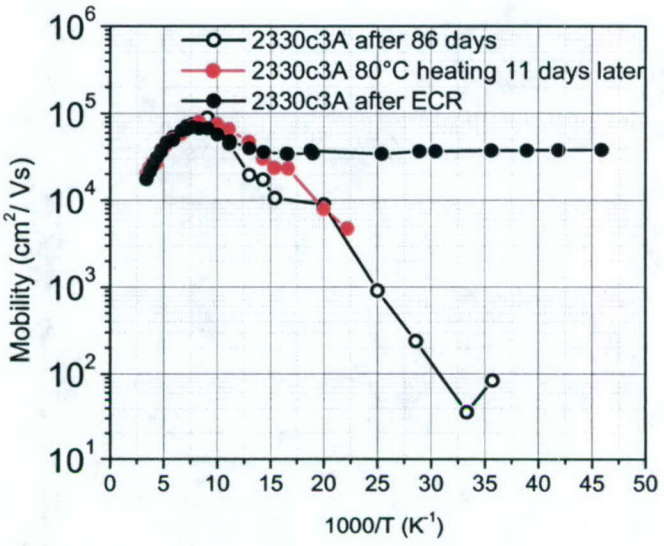

Figure 15. Hall mobilities measured 86 days apart for hydrogen passivated sample MCT02330c3. The red curve shows results from a measurement performed 11 days later, after heating the sample to 80°C.

In the case of sample MCT02330c3A, the transport properties change drastically over time. For the two lowest temperatures at which data are available, p-type conduction is observed and the effects of hydrogen passivation are lost, the sample reverting to conduction similar to that before ECR (see Figures 11 and 12, 425°C/235°C anneal). We conclude that hydrogen has left the Hg vacancies since this sample had a large number of Hg vacancies after annealing.

Figure 16 shows the minority carrier lifetimes for sample MCT02330c3A measured 54 days apart. The red curve shows data from the first measurements 78 days after ECR hydrogenation. The second measurement (black curve) was performed 3 days after the Hall measurements shown in Figures 14 and 15, a total of 132 days after ECR exposure.

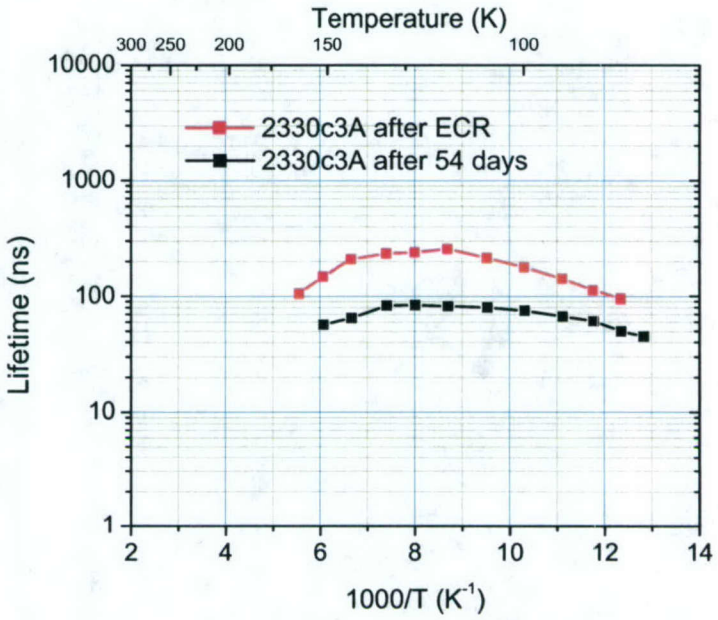

Figure 16. Temperature dependence of photoconductive minority carrier lifetimes measured 54 days apart for sample MCT02330c3A

Given the drastic change in the transport properties measured by Hall (Figures 14 and 15), suggesting that de-passivation of Hg vacancies may have taken place, the reduction in minority carrier lifetimes seen in Figure 16 is not unexpected. We believe that it is due to the reactivation of Hg vacancies as recombination centers. We cannot reach a conclusion regarding the stability of hydrogen passivating dislocations from this sample.

Samples from wafer MCT02331

Figures 17 and 18 show the Hall electrical carrier concentrations and mobilities for the samples from wafer MCT02331. The measured temperature dependences of the Hall constants are shown in Figure 19.

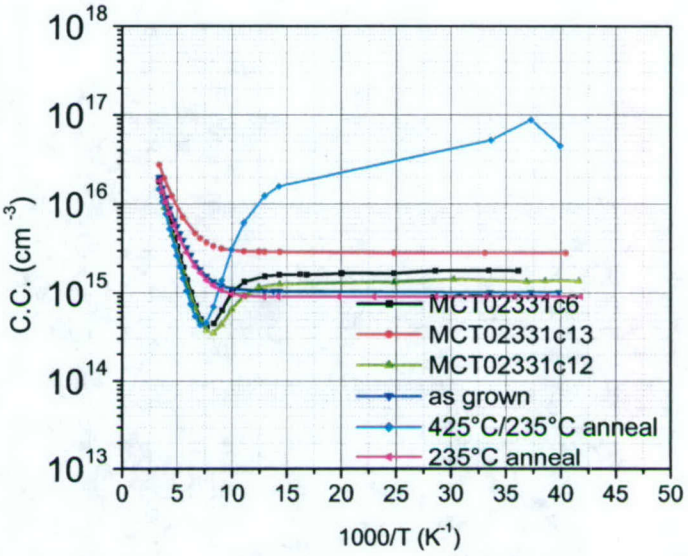

Figure 17. Hall carrier concentrations for samples from wafer MCT02331

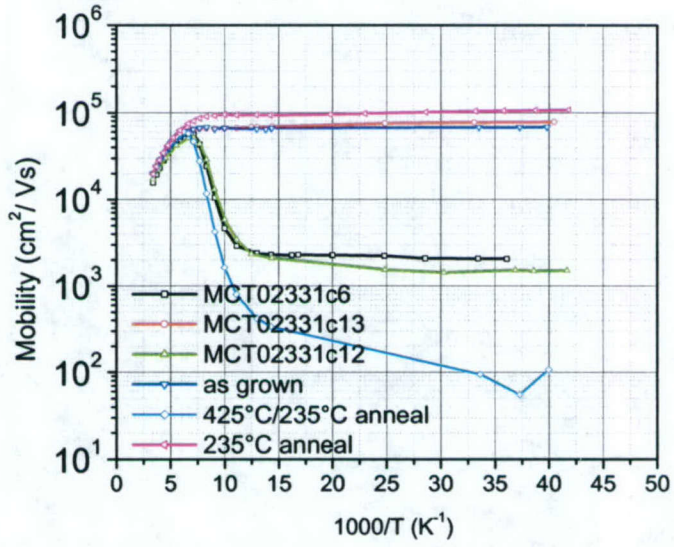

Figure 18. Hall mobilities for samples from wafer MCT02331

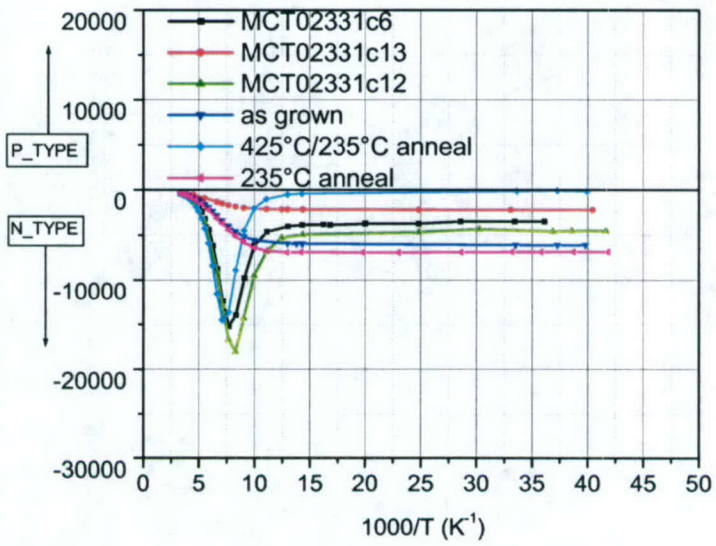

Figure 19. Hall constants Rh for samples from wafer MCT02331

Figures 20 and 21 show the carrier concentrations and mobilities of sample MCT02331c13 measured 60 days after the first Hall measurements and a total of 109 days following the ECR exposure. In addition to shelf storage, the heating of this sample to 80°C for 40 min. was performed 11 days after the second Hall measurement, a total of 120 days after ECR exposure. Hall measurement results following these experiments are also shown in Figures 20 and 21.

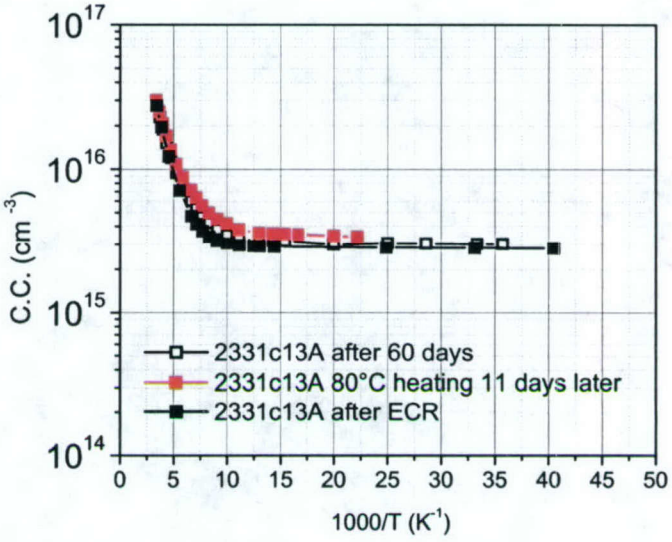

Figure 20. Hall electrical carrier concentrations measured 60 days apart for hydrogen passivated sample MCT02331c13. The red curve shows results from a measurement performed 11 days later, after heating the sample to 80°C

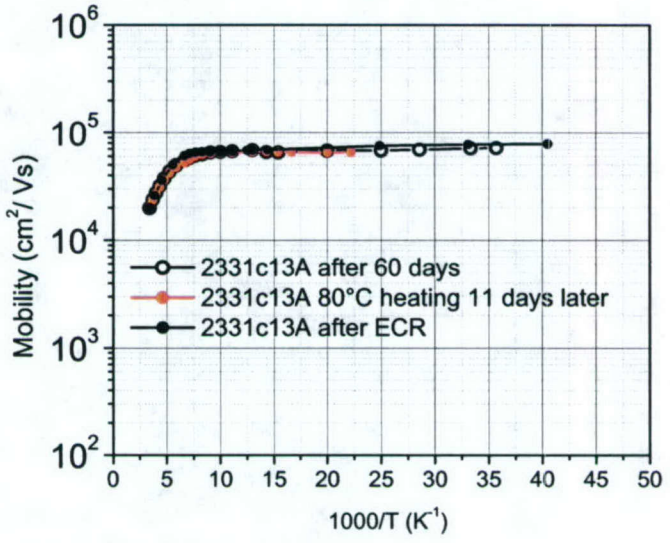

Figure 21. Hall mobilities measured 60 days apart for hydrogen passivated sample MCT02331c13. The red curve shows results from a measurement performed 11 days later, after heating the sample to 80°C

In the case of sample MCT02331c13A, no changes in the transport properties are noticed either after a period of storage or after heating the sample at 80°C. This is

certainly a very promising result which leads us to believe that hydrogen passivation can be maintained both during basic device processing and also during storage.

Samples from wafer MCT02333

Figures 22 and 23 show the Hall carrier concentrations and mobilities for the samples from wafer MCT02333. The measured temperature dependences of the Hall constants are shown in Figure 24.

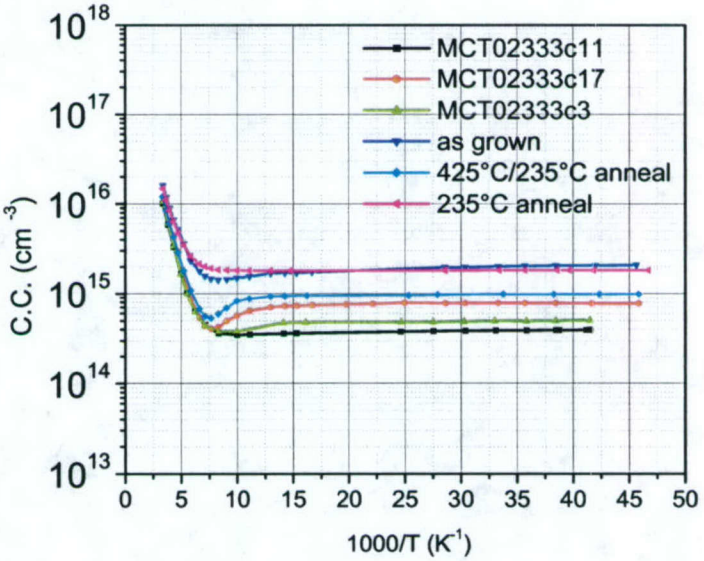

Figure 22. Hall carrier concentrations for samples from wafer MCT02333

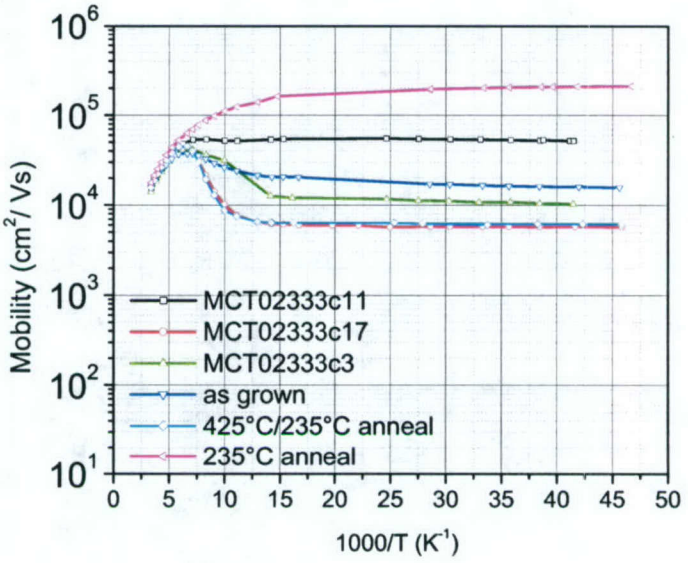

Figure 23. Hall mobilities for samples from wafer MCT02333

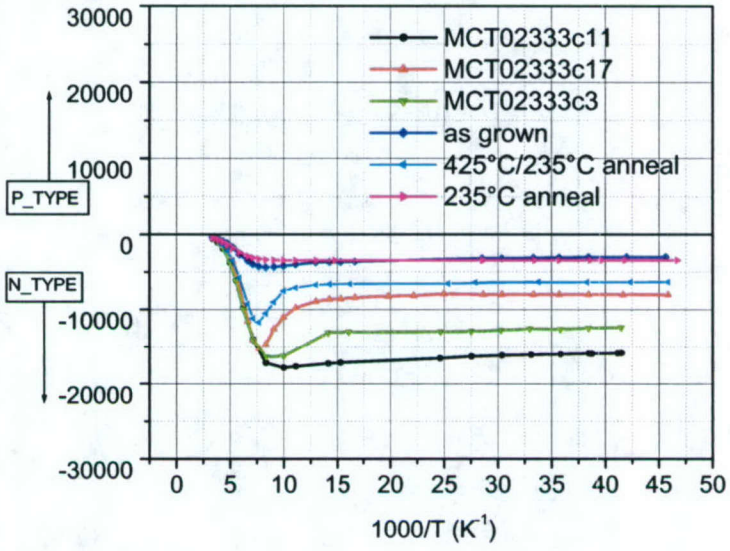

Figure 24. Hall constants Rh for samples from wafer MCT02333

Figure 25 shows the temperature-dependent recombination lifetime data for ECR exposed sample MCT02333c3. As a reference, lifetime data for a sample from the same wafer that was only annealed but not exposed to ECR is also plotted.

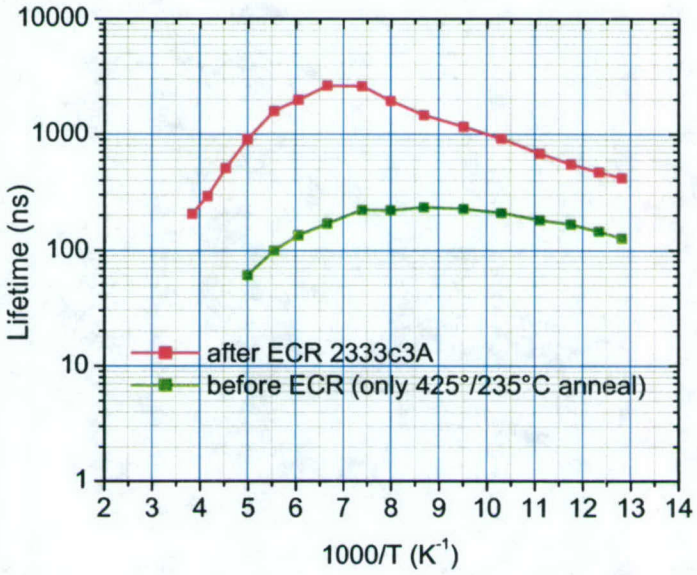

Figure 25. Electrical carrier lifetime for samples MCT02333c3A and MCT02333_HT

A one order of magnitude improvement in the minority carrier lifetimes was observed for ECR-exposed sample MCT02333c3A with respect to the reference sample (MCT02333_HT) that was annealed in the same way but not ECR-exposed. We note that this sample was chosen to not be of the highest quality, as indicated by the relatively short recombination lifetimes. This choice was made to reveal the maximum possible effects of hydrogenation. Note also that any surface or interface recombinations would only reduce the lifetime values, so the bulk carrier lifetimes must have been improved by an even larger factor than that measured. The results of these measurements are very encouraging since they confirm our expectation that hydrogen can be used to passivate recombination centers and hence increase minority carrier lifetimes.

Figures 26 and 27 show the carrier concentrations and mobilities for sample MCT02333c3 measured 41 days after the first Hall measurement and a total of 98 days following the ECR exposure.

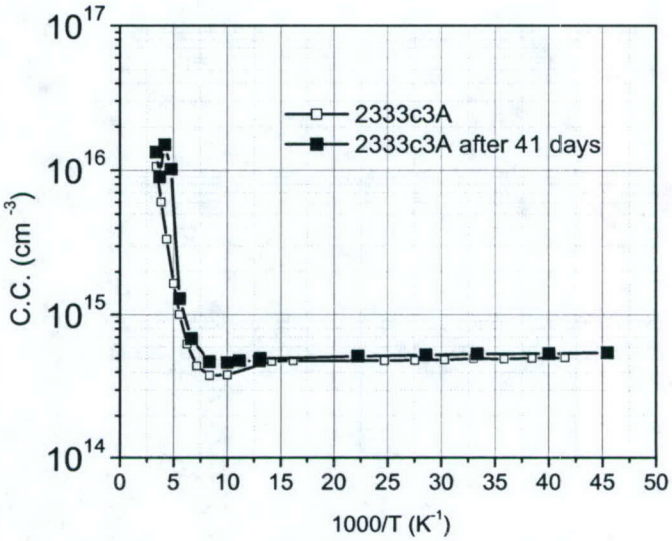

Figure 26. Hall electrical carrier concentrations measured 41 days apart for hydrogen passivated sample MCT02333c3

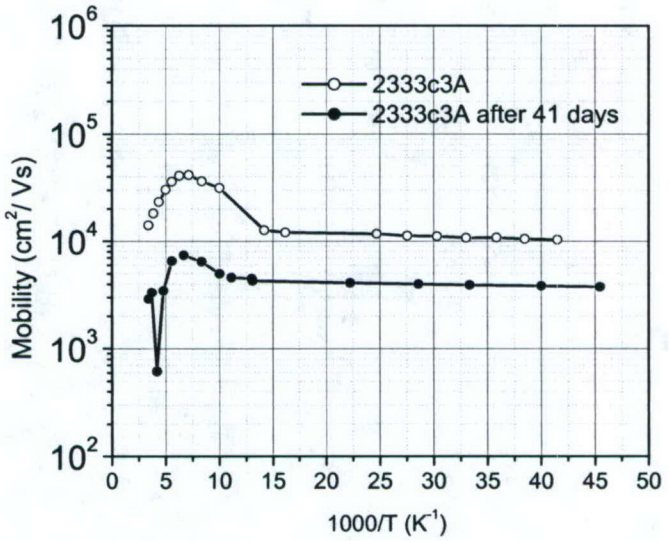

Figure 27. Hall mobilities measured 41 days apart for hydrogen passivated sample MCT02333c3

For sample MCT02333c3A, no significant changes are observed in the carrier concentrations measured at low temperatures after 41 days of storage; yet reduced carrier mobilities are evident, indicating an increase in the number of scattering centers. Lifetimes were measured for this sample and their temperature dependence is shown in Figure 28.

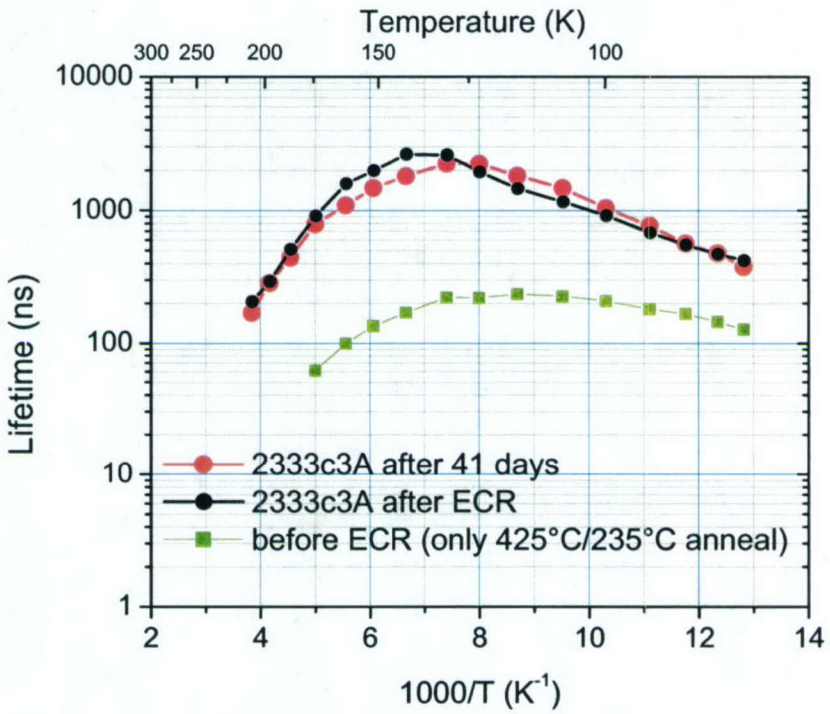

Figure 28. Temperature dependence of photoconductive minority carrier lifetimes measured 41 days apart for sample MCT02333c3.

No significant differences are observed between the red and black curves, indicating the stability of recombination center passivants. At this moment it is not clear why the Hall measurements (Figures 27) show a reduced mobility for essentially the same carrier concentrations and lifetimes after storage. These measurements will be redone to test the results.

Figure 29 shows the temperature-dependent recombination lifetime data for ECR exposed sample MCT02333c11A.

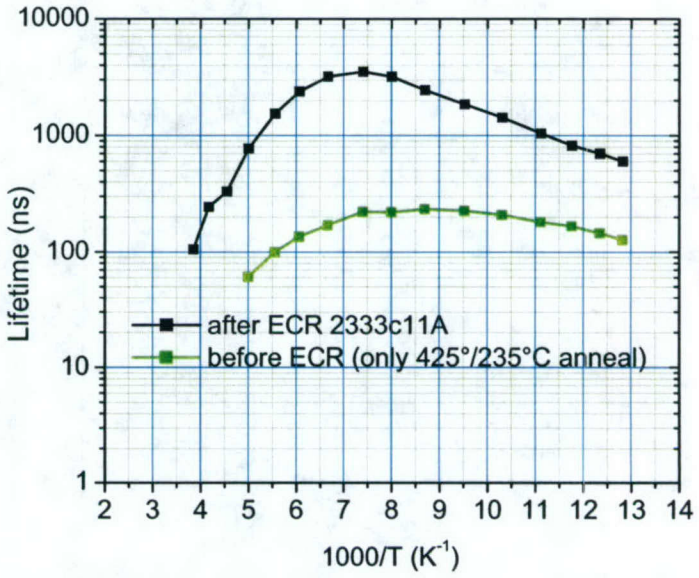

Figure 29. Electrical carrier lifetime for samples MCT02333c11A and MCT02333_HT

In this case, also, we noticed again a one order of magnitude improvement in the minority carrier lifetimes for ECR-exposed sample MCT02333c11A with respect to the reference sample (MCT02333_HT) that was annealed in the same way but not ECR-exposed.

Figures 30 and 31 show the carrier concentrations and mobilities for sample MCT02333c11A measured 48 days after the first Hall measurement and a total of 108 days following the ECR exposure. Figure 32 shows the temperature dependence of the Hall constant for the sample. As a reference, previously measured Hall results are also plotted.

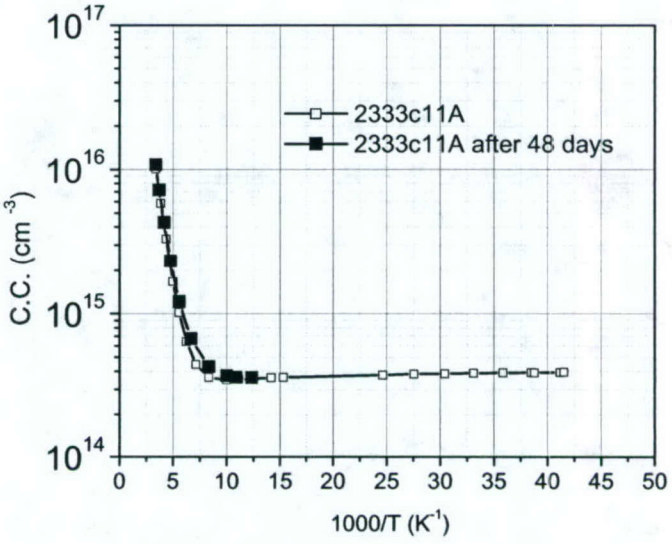

Figure 30. Hall electrical carrier concentrations measured 48 days apart for hydrogen passivated sample MCT02333c11

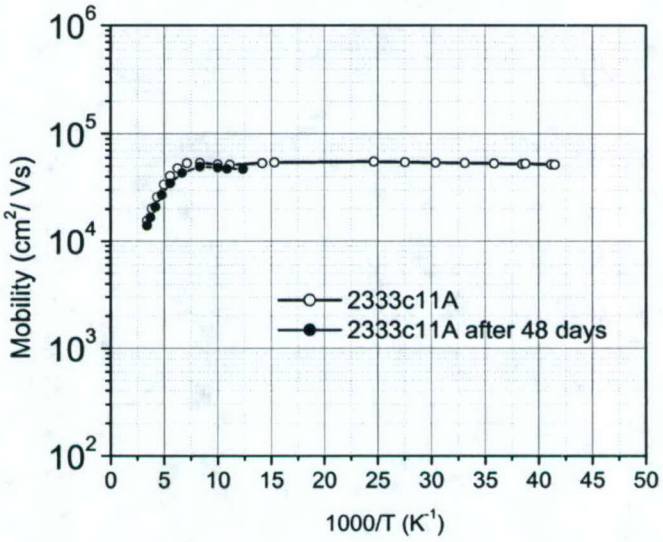

Figure 31. Hall mobilities measured 48 days apart for hydrogen passivated sample MCT02333c11

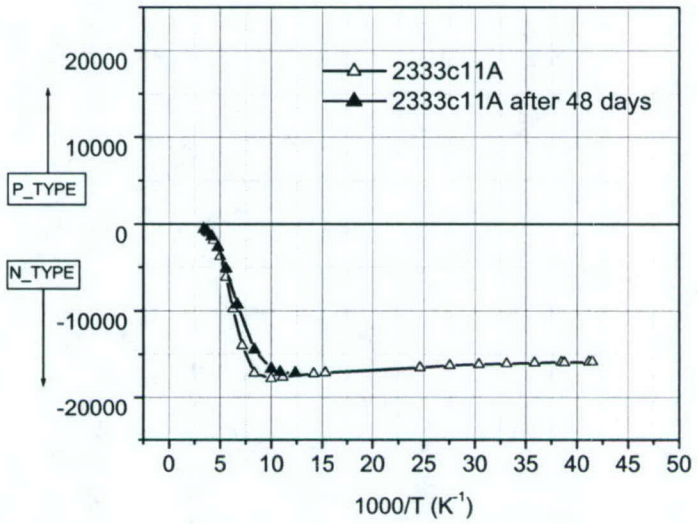

Figure 32. Hall constants measured 48 days apart for hydrogen passivated sample MCT02333c11

We do not see significant differences between the two sets of data over temperatures for which data is available, suggesting that sample aging does not affect the scattering mechanisms.

Figure 33 shows the minority carrier lifetimes measured after 27 days from the first measurement and 116 days since ECR exposure. The results of the first measurements as well as the lifetimes of a reference sample (to assess the "before ECR" status) are also shown in Figure 33.

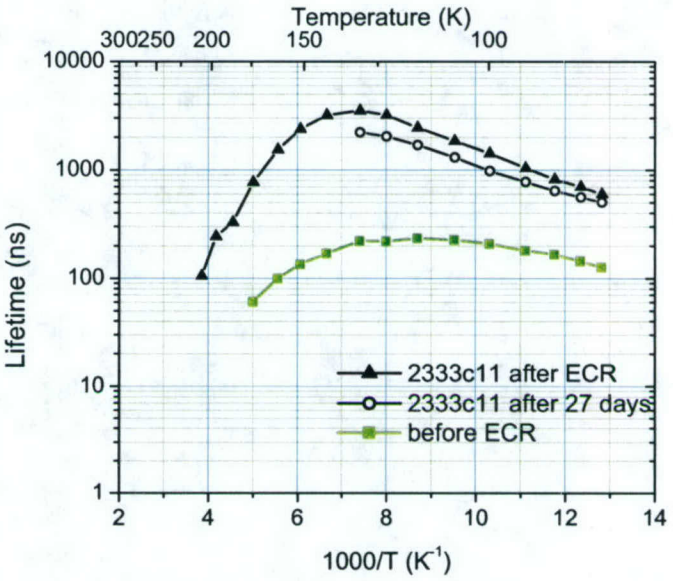

Figure 33. Temperature dependence of photoconductive minority carrier lifetimes measured 27 days apart for sample MCT02333c11

A small decrease of the lifetimes is noticed after shelf storage. This is still an encouraging result since the degradation in the measured carrier lifetimes is slight compared with the one order of magnitude improvement introduced by hydrogenation. Note that we used the same contacts as for the first measurements and no surface preparation was performed prior to the second measurements. The degradation could be due to the loss of some of the hydrogen passivants, but other effects such as surface degradation or contact degradation may be responsible.

Figures 34 and 35 show the carrier concentrations and mobilities for sample MCT02333c17 measured 73 days after the first Hall measurements and a total of 110 days following the ECR exposure.

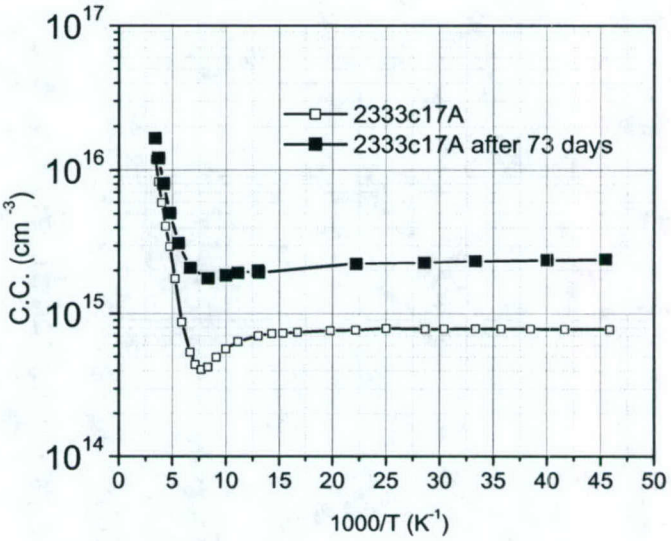

Figure 34. Hall electrical carrier concentrations measured 73 days apart for hydrogen passivated sample MCT02333c17

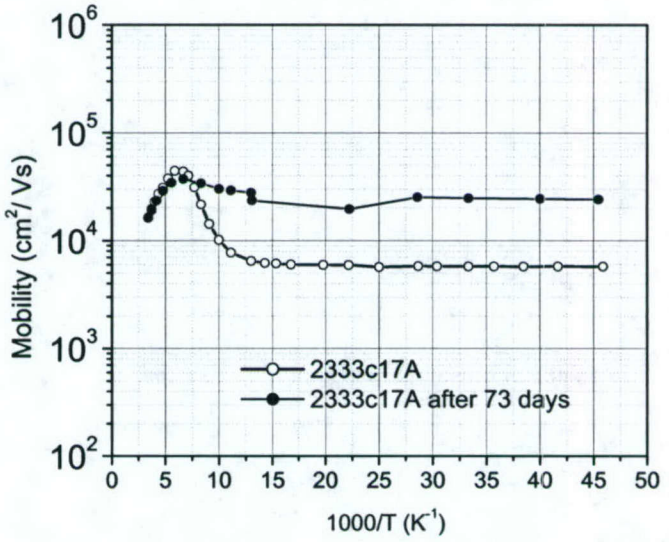

Figure 35. Hall mobilities measured 73 days apart for hydrogen passivated sample MCT02333c17

For this sample, we notice an improvement in carrier mobilities with aging and an increase in carrier concentrations. This could indicate that electrically active centers such as Hg vacancies were neutralized over time. The ECR exposure was limited to 1 min. for this sample and no significant differences were noticed in Hall measurements before and

after ECR. Nevertheless, hydrogen may have incorporated and further diffused into the sample during the storage period. It is not clear if this mechanism is responsible for the apparent passivation, since in another samples from the same wafer (MCT0233c3A) we noticed a possible de-passivation taking place, explained by perhaps hydrogen leaving the sample, and for one sample (MCT02333c11A) we do not notice any aging effects.

Given the complexity of the transport and recombination mechanisms that depend on a variety of defect types that could be affected to different extents by hydrogen, it is not surprising to see different interpretations of data for only a few samples. It is encouraging to have seen no deterioration of transport and lifetime properties of some samples after relatively long storage periods and heating, and we believe this recommends future efforts to fully elucidate the stability of hydrogen passivation.

Conclusions

During this Phase I effort, we demonstrated that ECR plasmas can introduce hydrogen into LWIR HgCdTe on Si with resulting improvements in key electrical parameters. Hall mobility and minority carrier lifetime data indicate that the incorporated hydrogen passivates both scattering and recombination centers when appropriate ECR conditions are used. While not fully understood, let alone optimized, the ECR parameters used so far produced results that lead us to believe that the use of hydrogen-only plasmas with an additional sample bias and a sample temperature of approximately 60°C increase the incorporation of hydrogen. While a protective ZnS layer preserved the surface morphology of HgCdTe samples, it peeled off in most cases during subsequent processing. Samples exposed to ECR plasmas that were not coated with ZnS contain a larger amount of hydrogen, with concentrations above the $1x10^{16}$ cm^{-3} detection limit of SIMS.

During this program, we found that dislocations play a role in atomic diffusion processes, both out-diffusion, observed during annealing, and in-diffusion of hydrogen during ECR exposures. This is why we believe that the passivation of dislocations is responsible for the increases in mobilities and minority carrier lifetimes following hydrogenation. Preliminary stability studies were performed on samples that were shelf-stored for more than a month and briefly heated, and indicate that hydrogenation of dislocations does not appear to be a reversible process over this period.

Should a Phase II be awarded, we will survey in greater detail the hydrogenation parameters and further test the stability of bulk passivation with hydrogen. We also intend to fabricate and test hydrogenated mesa and planar photodiodes, and focal plane arrays.

References

[1] Y. Dong, R.M. Feenstra, D.W. Greve, J.C. Moore, M.D. Sievert, and A.A. Baski, Appl. Phys. Lett. **86**, 121914 (2005).

[2] Y.F. Chen, C.S. Tsai, Y.H. Chang, Y.M. Chang, T.K. Chen and Y.M. Pang, Appl. Phys Lett. **58**, 493 (1991).

[3] A.P. Jacobs, Q.X. Zhao, M. Willander, T. Baron and N. Magnea, J. Appl. Phys. **90**, 2329 (2001).

[4] H.Y. Lee, T.W. Kang and T.W. Kim, J. Mater. Res. **16**, 2196 (2001).

[5] A.I. Evstigneev, V.F. Kuleshov, G.A. Lubochkova, M.V. Pashkovskii, E.B. Yakimov, and N.A. Yarkin, Sov. Phys. Semicond. **19**, 562 (1985).

[6] S.P. Komissarchuk, L.N. Limarenko, and E.P. Lopatinskaya in *Narrow Gap Semiconductors and Semimetals* (LVOV, Moscow, 1983) p. 126.

[7] H. Jung, H. Lee and C. Kim, J. Electron. Mater. **25**, 1266 (1996).

[8] Y. Kim, T. Kim, D. Redfern, C. Musca, H. Lee and C. Kim, J. Electron. Mater. **29**, 859 (2000).

[9] J.K. White, C.A. Musca, H.C. Lee, and L. Faraone, Appl. Phys. Lett **76**, 2448 (2000).

[10] S. H. Shin, J. M. Arias, D. D. Edwell, M. Zandian, J. G. Pasko, and R. E. DeWames, J. Vac. Sci. Technol. B **10**, 1492 (1992).

[11] V. Gopal and S. Gupta, J. Appl. Phys **95**, 2467 (2004).

[12] K. Yang, Y. Lee and H. Lee, Jap. J. Appl. Phys. **43**, L1617 (2004).

[13] M. Carmody, J.G. Pasko, P.D. Edwall, M. Daraselia, L.A. Almeida, J. Molstad, J.H. Dinan, J.K. Markunas, Y. Chen, G. Brill, and N.K. Dhar, J. Electron Mater. **33**, 531 (2004).

[14] X.Y. Sun, R. Bommena, D. Burckel, A. Frauenglass, M.N. Fairchild, S.R.J. Brueck, G.A. Garrett, M. Wraback, and S.D. Hersee, J. Appl. Phys. **95**, 1450 (2004).